

Aging and memory of transitional turbulence

Vasudevan Mukund, Chaitanya Paranjape, Michael Philip Sitte, and Björn Hof*

IST Austria

(Dated: December 14, 2021)

The recent classification of the onset of turbulence as a directed percolation (DP) phase transition has been applied to all major shear flows including pipe, channel, Couette and boundary layer flows. A cornerstone of the DP analogy is the memoryless (Markov) property of turbulent sites. We here show that for the classic case of channel flow, the growth of turbulent stripes is deterministic and that memorylessness breaks down. Consequently turbulence ages and the one to one mapping between turbulent patches and active DP-sites is not fulfilled. In addition, the interpretation of turbulence as a chaotic saddle with supertransient properties, the basis of recent theoretical progress, does not apply. The discrepancy between channel flow and the established transition model illustrates that seemingly minor geometrical differences between flows can give rise to instabilities and growth mechanisms that fundamentally alter the nature of the transition to turbulence.

Many stochastic processes such as radioactive decay or the inter-arrival times of new bitcoin blocks are memoryless, i.e. the probability of an event to occur is constant in time. Fluid flows on the other hand are governed by deterministic equations, and the flow state at an instance in time in principle fully determines the entire future evolution. It may therefore come as a surprise that the transition to turbulence in a large number of flows is governed by memoryless processes. This seemingly contradictory state of affairs is reconciled by the sensitive dependence on initial conditions — a defining property of deterministic chaos that equally applies to turbulent fluid motion. The associated exponential amplification of even minute differences makes long term forecasts of the dynamics impossible in practice, and effectively erases the flow's memory.

It is precisely this memoryless property that has paved the way for a possible solution to the century old puzzle surrounding the nature of the transition to turbulence. More specifically, the transition in Couette, pipe and related shear flows is characterized by the co-existence of laminar and turbulent regions. Such patches of turbulence, although frequently long lived, are transient, and their decay is abrupt and unpredictable — more precisely, memoryless. The underlying dynamical-systems model is that of a chaotic saddle in phase space [1], and the laminar state corresponds to an attracting fixed point, where the escape rate from the former is constant in time [2]. This is probably the best established property of transitional turbulence in subcritical shear flows, and a large body of literature (e.g.[3–14]) has been dedicated to the dynamical-systems aspects, including studies of the underlying exact coherent structures[1, 15–17], the boundary crisis [18–22] that gives rise to transient chaos, and the resulting edge state that mediates the eventual escape from turbulence [23, 24]. Corresponding transient dynamics have equally been observed for turbulence in astrophysical accretion discs[25], in nonlinear fibre optics[26], for the dynamo transition in magnetohydrodynamic turbulence[27], turbulence in pulsatile[28] (e.g. cardiovascular) flows and surprisingly even extend to the generic case of isotropic turbulence[13].

In addition to the temporal dynamics, also the spatial proliferation, i.e. the nucleation of new patches via a contact process (called ‘puff splitting’ [29] in pipes), turned out to be memoryless [30]. These combined insights have not only allowed to determine the critical point for the onset of sustained turbulence [30], but also led to a direct analogy to non-equilibrium phase transitions and in particular to directed percolation (DP): individual patches of turbulence can be interpreted as active sites which just like in models of DP can

either decay or infect their neighbours, and the probability for either event to take place does not depend on time. Based on these insights, DP is believed to be the standard route to turbulence for this entire class of flows [31–36]. Moreover these concepts have been applied to the dynamics of active biological matter [37] as well as to the Leidenfrost effect[38] in soft matter physics where starting from observations of Markovian structures (analogous to puffs) DP exponents have been measured.

At first sight, channel flow perfectly complies with all of the above criteria. In the transitional regime, turbulence appears in the form of stripes, and simulations in periodic boxes confirmed the memoryless nature of decay and splitting of individual stripes [14, 39, 40]. Like in other shear flows [30, 31], the critical point has been approximated by comparing mean life and splitting times [39]. Additionally, an experimental study [33] suggested that the onset of sustained turbulence falls into the DP universality class seemingly explaining the nature of this transition. A closer look at the latter study however reveals that the time scales resolved (~ 2400 advective time units) were more than 3 orders of magnitude shorter than those proposed in the DP analogy for pipe and Couette flow. Moreover the spot like flow structures formed during the short time scales of this experiment did not correspond to the large scale stripe patterns that are characteristic for transitional channel flows (e.g. see [41, 42] and Fig. 1). Finally as shown by a number of recent studies [41–44], the actual critical point where turbulent stripes first become sustained in channel flow is substantially lower than the critical point proposed by [33] and consequently these latter experiments were carried out far from the onset of sustained turbulence.

A model study, attempted to remedy the shortcomings of these channel experiments by suggesting that at the actual (i.e. much lower) critical point the transition may fall into the 1+1D DP universality class and crosses over to 2+1 D DP further from critical [42, 44]. On the other hand, a numerical study of nonlocalized stripes in periodic domains [39] reported that the characteristic time scales for the decay and the nucleation of new stripes exceed 10^6 advective time units at the critical point. While it is not clear if the decay and proliferation of fully localised stripes follow the same rules, such excessive time scales would put a characterisation of the nature of the transition practically beyond reach.

We will show in the following that stripe localization a process intrinsic to transitional channel flow, fundamentally alters the proliferation and decay processes of turbulence. Unlike for other shear flows, stripes in channel flow become sustained via a deterministic

growth process. Even close to the critical point, and over the longest observation times realizable, turbulent stripes are not memoryless, the critical point cannot be approximated in the standard way [30], the common edge tracking routine does not converge and the aforementioned mapping of turbulent stripes to DP sites does not hold.

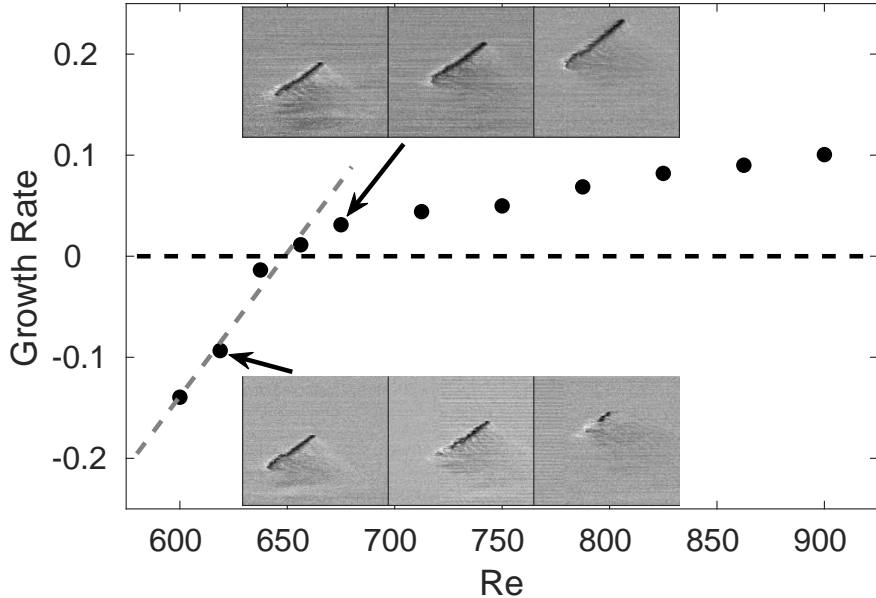


FIG. 1: Transition from shrinking to expanding turbulent stripes. The mean growth rate of turbulent regions is plotted as a function of Re . The first 4 points are fitted by a straight line to estimate the Re at which the growth rate first becomes positive, which is $Re \sim 650$. Above this Re , individual stripes grow, while below, they eventually decay, as seen in the insets showing a sequence of flow visualisation images.

Experiments are carried out in a large aspect ratio channel, considerably exceeding domain sizes of most earlier studies. Specifically, the channel's dimensions are $(Lx; Ly; Lz) = (4000h; 2h; 490h)$, where Lx , Ly and Lz are lengths in the streamwise, wall-normal and spanwise directions respectively. Quantities are non-dimensionalised with the length scale h (half-gap) and 1.5 times the bulk velocity u_b (corresponding to the centre-line velocity in case of laminar flow). In keeping with numerical and theoretical studies, we define the Reynolds number as $Re = 1.5u_bh/\nu$, where ν is the kinematic viscosity. Unless perturbed, the flow stays laminar over the entire Reynolds number range investigated.

We used two protocols to obtain isolated stripes. Stripes were created either by perturbing the flow across a certain width ($\sim 20h$ in the spanwise direction) or a stripe was thus created

at a higher flow-rate, followed by a quench to the target Re . The latter mechanism was found to be more efficient at lower Re , at which the former creates stripes only sporadically. At Re where both mechanisms work well, results are qualitatively the same regardless of the perturbation type, provided that the created stripes are of comparable size.

Turbulent stripes are investigated in the range $600 \leq Re \leq 900$. For each Re , around 1000 individual stripes are generated near the channel entrance.

As they advect downstream, they are monitored by multiple cameras along the channel, until they eventually exit the channel. More details are available in the Supplementary Information. Note that in all the experiments, stripes remained at a minimum distance of $50h$ from the lateral boundaries and stripe advection velocities and tip speeds remain unchanged up to this point indicating that stripes are unaffected by the side walls. Overall more than 10,000 stripes are tracked in order to obtain reliable statistics and the total observation time exceeds 5×10^7 advective time units. The resulting images are analysed to extract various quantities of interest. In particular, the area occupied by turbulence is determined as a function of time and used to compute the mean growth rate of turbulence, which is shown in Fig.1. For $Re \lesssim 650$, growth rates are negative, while above this Re , the growth rate becomes positive and continues to increase with Re . We propose that once individual stripes continuously grow also turbulence as a whole will eventually cease to decay and hence the critical point for channel flow can be estimated to be $Re_c \approx 650$. In agreement with recent numerical studies [41–44] our experiments also confirm that the critical point is significantly lower than that reported by [33].

In order to characterize the decay of turbulence below the critical point, we next investigate stripe lifetimes at $Re = 600$, i.e. $\sim 8\%$ below Re_c . Fig 2a shows the probability that a stripe survives until a time t . It is apparent from Fig. 2a (red dots) that survival probabilities do not follow the exponential distribution that characterizes a memoryless process, and would equally be expected for the statistics of DP sites. For comparison we show puff lifetimes [11] for pipe flow at $Re = 1900$, $\sim 7\%$ below Re_c and at an even lower value of $Re = 1860$, $\sim 9\%$ below critical, and both data sets (grey symbols) clearly follow exponential distributions characteristic for a chaotic saddle. In channel flow on the other hand, even upon a closer approach to critical ($Re = 620$, $\sim 5\%$ below Re_c), stripe lifetimes (Fig. 2a, red triangles) show no sign of memorylessness. In contrast to puffs, the decay rate of localized stripes is not constant: No decays are found during a long initial phase, that grows as the

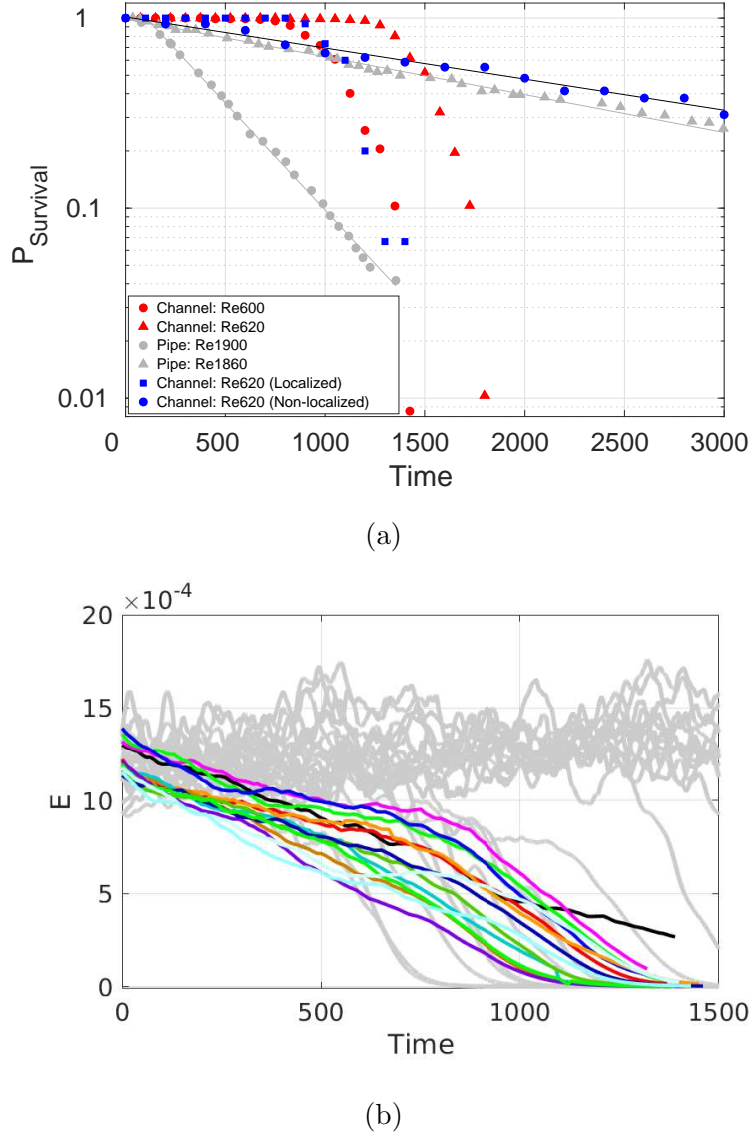


FIG. 2: **Aging of stripes.** Panel (a) shows the survival probability of turbulent structures in pipe and channel flow. Non-localized stripes from DNS (blue dots), show the expected exponential drop in survival probabilities signifying a memoryless decay similar to puffs in pipe flow (grey symbols, data taken from [11]). Natural, i.e. fully localized stripes in experiments (red circles and triangles) or DNS (blue squares) show aging, i.e a decay process that is not memoryless, as seen by survival probabilities that are clearly not exponential. (b) Evolution of turbulent kinetic energy of stripes in direct numerical simulations. In moderate domains (grey curves) where stripes cannot localize the decays occur at unpredictable times. Fully localised stripes (coloured curves) show a continuously decreasing energy and decays occur at comparable times.

critical point is approached (~ 900 advective time units at $Re = 600$, ~ 1300 advective time units at $Re = 620$). Subsequently all stripes decay in a comparably short time interval (within ~ 500 advective time units). It is also apparent from Fig. 2a that the tail of the respective distribution (red stars and red triangles) does not approach a constant slope but continues to steepen down to the lowest probabilities measurable. While initial transient periods are known for pipe flow[7], these are however only of order 100 advective time units and mark the period during which the puff forms (t_0). In our channel experiments the stripes are already fully formed from the start and subsequently undergo a slow aging process and as will be shown below, during this phase, the stripe recreation, or more precisely the streak production rate, slows down.

The shape of the lifetime distributions do not only fundamentally differ from those in pipe and Couette flows [7, 31], but surprisingly also from computations of channel flow in small domains. In such computational boxes stripes cannot fully localize and are found to be memoryless [14, 39]. To verify these computational studies, we carried out direct numerical simulations in a long yet slender channel (30h; 2h; 100h) that is tilted by 45° , the same angle that stripes naturally assume with respect to the mean flow; see Supplementary Information for details. This method [45] ensures that stripes, just like in previous numerical studies, connect via the periodic boundary, and hence localization is prohibited. Just like observed in earlier simulations, such periodic stripes have exponentially distributed lifetimes and are hence memoryless (blue dots in Fig. 2a). However when the computational domain size is increased (400h; 2h; 400h) to allow stripes to fully localize and assume their natural shape, the memoryless nature disappears and stripes age, confirming the experimental observation. As shown in Fig. 2a (blue squares), at $Re = 620$, localised stripes do not decay for the first ~ 900 advective time units, but all of them disappear within a subsequent interval of ~ 500 time units, in excellent qualitative agreement with our experiments. In addition to whole stripes we can also partition stripes and determine the survival probability of stripe segments (i.e. a fixed number of streaks within a stripe), and in this case as well the corresponding distributions are not memoryless.

It should also be noted that for such aging processes, the time of decay and hence the lifetime depends on the energy threshold chosen. This becomes evident from the energy time-series of stripes, shown in Fig. 2b for $Re = 620$. Non-localised stripes (grey lines) show a well defined energy plateau for turbulence and decays can happen at any time with equal

probability. In contrast, localised stripes (coloured lines) age, exhibiting a gradual energy decay. The time of the decay is not clearly defined and depends on the energy cut off chosen (as shown in Supplementary Fig.4) which however does not affect the qualitative shape of the distributions. The lack of a clear energy plateau also makes standard bisection methods [24, 46], commonly used to track the edge between laminar and turbulent flow, unsuitable.

In order to determine if closer to critical, stripe decays may be memoryless, we conducted experiments at $Re = 640$. However here, virtually no stripe decays could be observed over the length of the channel. Even after increasing the number of investigated stripes to more than 1000, no decay was detected, despite the fact that overall stripes were shrinking in size. Hence, the aging time appears to have increased beyond the advection time through the channel. For memoryless decays, limitations in the domain length can simply be compensated by an increase in the number of cases investigated (e.g. as carried out by [30]), this is however not applicable if structures age like in the present case.

We next investigate the proliferation of stripes slightly above the critical point, at $Re = 655$. As shown in Fig. 3a, stripes do not just passively advect downstream but at the same time move across the channel, i.e. in the spanwise direction. The spanwise motion is caused by the continuous creation of streaks at the downstream tip (see Fig.3c and movie in the Supplementary Information). Unlike for growth processes in other shear flows (e.g. puff nucleation in pipe flow [30] and in particular also unlike for stripe growth in Couette flow [47]), here streaks are created at a constant rate (Fig. 3d) and this process is hence deterministic. This streak creation has recently been linked to a hydrodynamic instability particular to localized stripes in channel flow [48]. If the Reynolds number is decreased below critical, streaks are initially created at the same rate which results in an identical stripe migration speed (compare blue dashed lines in Fig. 3a and 3b). As long as this streak production mechanism is intact, stripes do not decay. However below critical, the production eventually slows down, and the tip speed decreases (the tip deviates from the blue dashed line in 3b). Consequently the stripe shrinks and eventually dies.

In contrast to the deterministic and constant growth at the stripe's downstream tip, the dynamics at the tail (i.e. upstream tip) is stochastic. Stripe segments of varying size split off and detach from the tail at irregular intervals. Some examples are marked by the red circles in Fig. 3a and 3b. The split pieces typically dissipate. However longer pieces occasionally survive and form a new stripe upstream and parallel to the parent stripe (see Supplementary

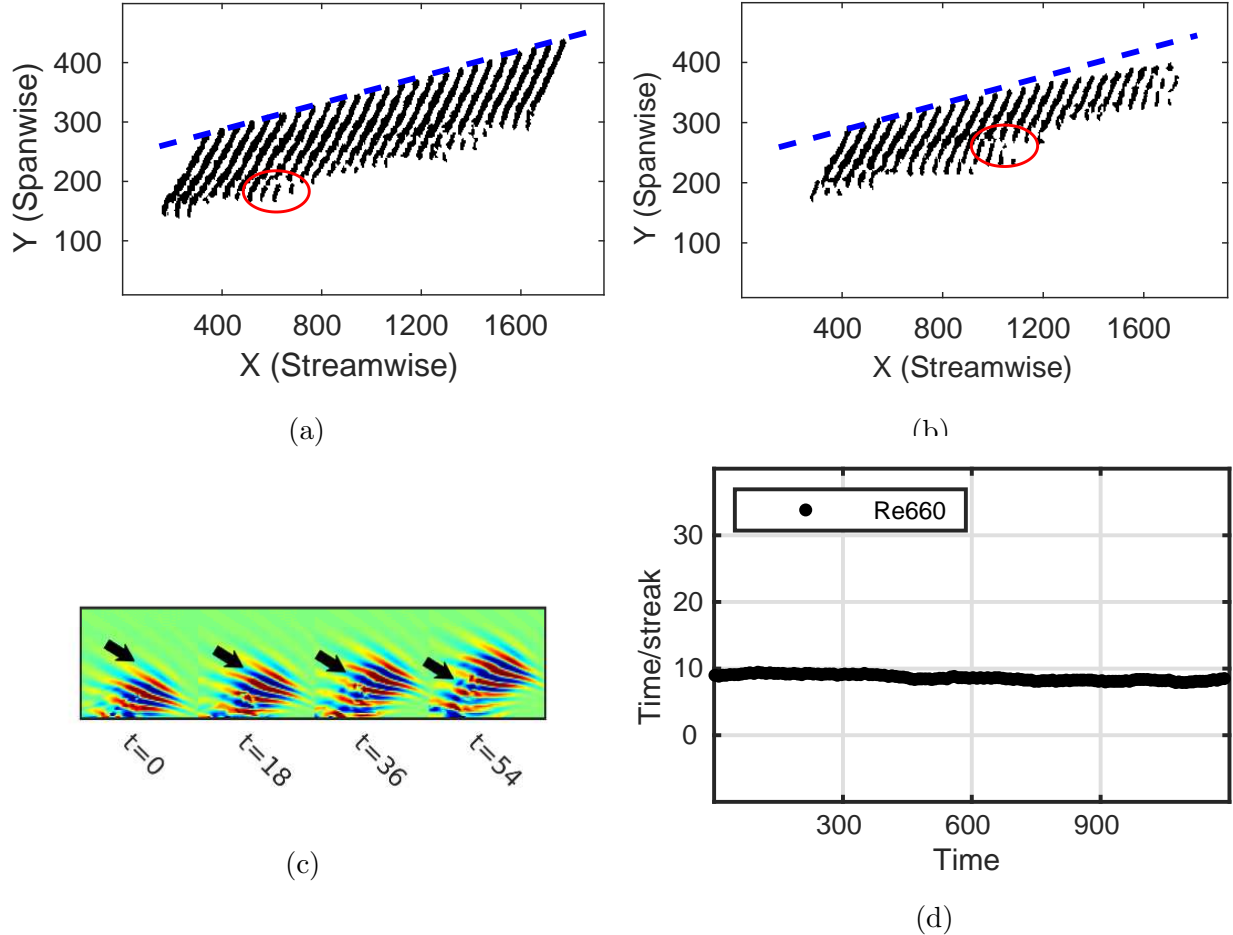


FIG. 3: **Deterministic stripe expansion and streak creation.** Panel (a) displays consecutive positions of a stripe at $Re = 655$. The downstream tip moves at a constant velocity diagonally across the channel as indicated by the dashed blue line, and laminar fluid is entrained at a constant rate (b) Below the critical point, at $Re = 620$, the tip initially moves with the same velocity as the stripe at $Re = 655$ but slows down in time and eventually the stripe decays. (c) Snapshots of the wall normal velocities in the region around the downstream tip of the stripe at $Re = 655$, obtained from DNS. showing a pair of streaks are created every ~ 18 advective time units. To more easily follow the addition of streaks, the streaks emerging in the first snapshot ($t=0$, arbitrary time origin) is shown with an arrow in all the subsequent snapshots (d) The time interval between the addition of two successive streaks shown as a function of time for $Re = 655$

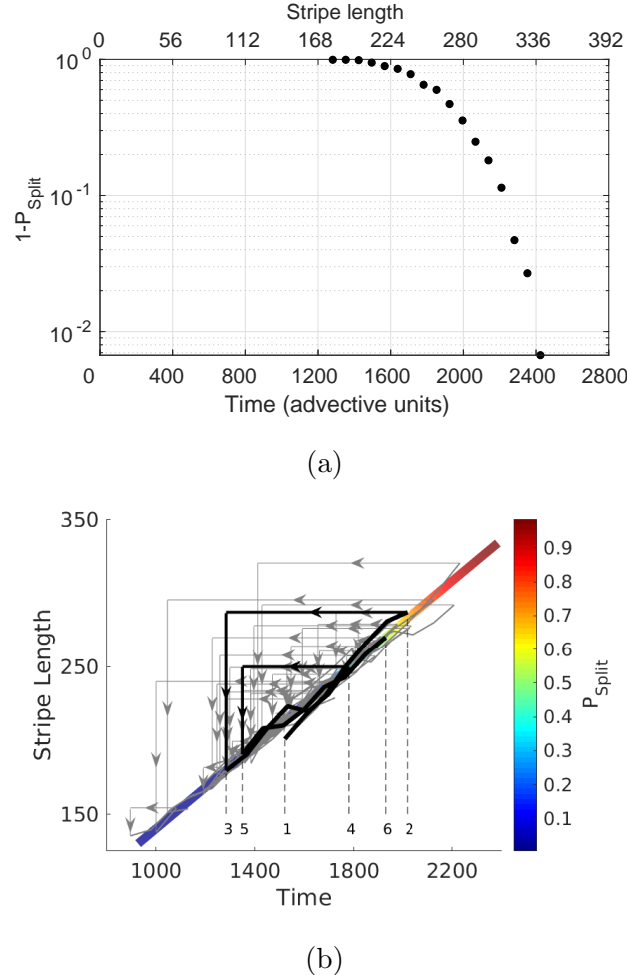


FIG. 4: **Age dependence of stripe splitting.** (a) Probability of a stripe not to split $1 - P_{split}$ till a time t , as a function of its time or age, showing a non-exponential tail (b) Stripes at $Re = 710$, a little above Re_c , exhibiting cycles of growth and splitting. The diagonal line indicates the growth of a stripe in absence of splitting, while the color gradient gives the probability for it to split, which increases with the length of the stripe. The gray curves give the evolution of the length of stripes with time, with one particular stripe shown in black. The horizontal and vertical arrows indicate splitting events which 'reset' a stripe's length and age. These events are numbered for the stripe shown in black - see text for details. After such splitting events, the stripe grows till a further splitting and so on, establishing a cycle of growth and splitting. Note that here only splittings of stripe segments larger than $20h$ are shown for clarity.

Fig.3 for an example). To quantify this, we look at the probability of splitting as a function of the stripe length. The constant growth rate of a stripe in between splittings can be used to convert the length into a time, which may be interpreted as the intrinsic time or age of a stripe, where time $t = 0$ corresponds to the extrapolated time where the stripe length is zero. The splitting statistics are shown in Fig.4a, where the probability of a stripe to stay intact (i.e not split) is shown as a function of length / age of the stripe. Stripes shorter than 200h have a splitting probability close to zero. However as time proceeds and their lengths continue to increase, stripes appear to lose their structural stability and the probability to split increases, resulting in a non-exponential tail in Fig 4a. Thus, also stripe splitting is not memoryless, but an aging process.

The coupling between the growth of a stripe and its splitting probability leads to a cyclic process depicted in Fig. 4b. The length evolution is shown for several randomly chosen stripes (grey curves) at $Re = 710$. A representative stripe is highlighted in black. Starting from point 1 it initially grows at a constant rate (diagonal line in Fig. 4b), driven by the addition of streaks at the downstream tip. With the stripe's length also its probability to split increases (shown by the color gradient) and in this case the splitting eventually occurs at point 2. Splitting resets this stripe to a shorter length (point 3) which can be interpreted as a younger stripe age and the growth resumes until the next splitting occurs (point 4). The stripe is 're-set' to point 5, and grows until point 6 (at which point it exited the test section). Corresponding cyclic dynamics (light grey curves) are exhibited by all stripes regardless of initial conditions. The interplay between stripe elongation and splitting, causes the overall proliferation of turbulence to be two dimensional.

Aging dominates stripe dynamics below as well as above the critical point and both aspects are closely connected to the deterministic growth at the stripes' downstream tip, an aspect that is crucially missing in many previous studies of channel flow.

Memoryless stochastic dynamics is a defining characteristic of shear flow turbulence, It is a signature of the underlying chaotic saddle and in a spatio-temporal context this Markov property allows to link the problem to directed percolation. Many recent studies have confirmed this scenario suggesting its robustness. On the other hand examples from astrophysical and cardiovascular flows have shown that subtle geometrical changes and imperfections can entirely alter the flows' stability and the nature of the transition[49, 50]. In channel flow it is not imperfections but on the contrary the approach towards the classic problem's (i.e.

unconstrained) geometry which challenges the robustness of the transition model.

* bhof@ist.ac.at

- [1] B. Eckhardt, T. M. Schneider, B. Hof, and J. Westerweel, *Annu. Rev. Fluid Mech.* **39**, 447 (2007).
- [2] T. Tél and Y.-C. Lai, *Physics Reports* **460**, 245 (2008).
- [3] S. Bottin, F. Daviaud, P. Manneville, and O. Dauchot, *EPL (Europhysics Letters)* **43**, 171 (1998).
- [4] H. Faisst and B. Eckhardt, *Journal of Fluid Mechanics* **504**, 343 (2004).
- [5] J. Moehlis, H. Faisst, and B. Eckhardt, *New Journal of Physics* **6**, 56 (2004).
- [6] J. Peixinho and T. Mullin, *Physical review letters* **96**, 094501 (2006).
- [7] B. Hof, J. Westerweel, T. M. Schneider, and B. Eckhardt, *Nature* **443**, 59 (2006).
- [8] A. P. Willis and R. R. Kerswell, *Physical review letters* **98**, 014501 (2007).
- [9] B. Hof, A. de Lozar, D. J. Kuik, and J. Westerweel, *Physical review letters* **101**, 214501 (2008).
- [10] T. M. Schneider and B. Eckhardt, *Physical Review E* **78**, 046310 (2008).
- [11] M. Avila, A. P. Willis, and B. Hof, *Journal of Fluid Mechanics* **646**, 127 (2010).
- [12] D. Borrero-Echeverry, M. F. Schatz, and R. Tagg, *Physical Review E* **81**, 025301 (2010).
- [13] M. F. Linkmann and A. Morozov, *Physical review letters* **115**, 134502 (2015).
- [14] M. Shimizu, T. Kanazawa, and G. Kawahara, *Fluid Dynamics Research* **51**, 011404 (2019).
- [15] B. Hof, C. W. van Doorne, J. Westerweel, F. T. Nieuwstadt, H. Faisst, B. Eckhardt, H. Wedin, R. R. Kerswell, and F. Waleffe, *Science* **305**, 1594 (2004).
- [16] R. Kerswell, *Nonlinearity* **18**, R17 (2005).
- [17] G. Kawahara, M. Uhlmann, and L. Van Veen, *Annual Review of Fluid Mechanics* **44**, 203 (2012).
- [18] L. van Veen and G. Kawahara, *Physical review letters* **107**, 114501 (2011).
- [19] T. Kreilos and B. Eckhardt, *Chaos: An Interdisciplinary Journal of Nonlinear Science* **22**, 047505 (2012).
- [20] M. Avila, F. Mellibovsky, N. Roland, and B. Hof, *Physical review letters* **110**, 224502 (2013).
- [21] P. Ritter, F. Mellibovsky, and M. Avila, *New Journal of Physics* **18**, 083031 (2016).

- [22] N. B. Budanur, A. S. Dogra, and B. Hof, *Physical Review Fluids* **4**, 102401 (2019).
- [23] T. Itano and S. Toh, *Journal of the Physical Society of Japan* **70**, 703 (2001).
- [24] T. M. Schneider, B. Eckhardt, and J. A. Yorke, *Physical review letters* **99**, 034502 (2007).
- [25] E. L. Rempel, G. Lesur, and M. R. E. Proctor, *Physical review letters* **105**, 044501 (2010).
- [26] E. Turitsyn, S. Smirnov, S. Sugavanam, N. Tarasov, X. Shu, S. Babin, E. Podivilov, D. Churkin, G. Falkovich, and S. K. Turitsyn, *Nature Photon* **7**, 783 (2013).
- [27] E. L. Rempel, M. R. E. Proctor, and A. C. L. Chian, *Mon. Not. R. Astron. Soc.* **400**, 509 (2009).
- [28] D. Xu, S. Warnecke, B. Song, X. Ma, and B. Hof, *Journal of Fluid Mechanics* **831** (2017).
- [29] D. Moxey and D. Barkley, *Proceedings of the National Academy of Sciences* **107**, 8091 (2010).
- [30] K. Avila, D. Moxey, A. de Lozar, M. Avila, D. Barkley, and B. Hof, *Science* **333**, 192 (2011).
- [31] L. Shi, M. Avila, and B. Hof, *Physical review letters* **110**, 204502 (2013).
- [32] G. Lemoult, L. Shi, K. Avila, S. V. Jalikop, M. Avila, and B. Hof, *Nature Physics* **12**, 254 (2016).
- [33] M. Sano and K. Tamai, *Nature Physics* **12**, 249 (2016).
- [34] M. Chantry, L. S. Tuckerman, and D. Barkley, *Journal of Fluid Mechanics* **824** (2017).
- [35] Y. Hiruta and S. Toh, *Journal of the Physical Society of Japan* **89**, 044402 (2020).
- [36] D. Traphan, T. Wester, G. Gürkler, J. Peinke, and P. Lind, *Physical review X* **8**, 021014 (2018).
- [37] A. Doostmohammadi, T. N. Shendruk, K. Thijssen, and J. M. Yeomans, *Nature Communications* **8**, 15326 (2017).
- [38] P. Chantelot and D. Lohse, *Physical review letters* **127**, 124502 (2021).
- [39] S. Gomé, L. S. Tuckerman, and D. Barkley, *Physical Review Fluids* **5**, 083905 (2020).
- [40] L. S. Tuckerman, M. Chantry, and D. Barkley, *Annual Review of Fluid Mechanics* **52** (2020).
- [41] X. Xiong, J. Tao, S. Chen, and L. Brandt, *Physics of Fluids* **27**, 041702 (2015).
- [42] M. Shimizu and P. Manneville, *Physical Review Fluids* **4**, 113903 (2019).
- [43] J. Tao, B. Eckhardt, and X. Xiong, *Physical Review Fluids* **3**, 011902 (2018).
- [44] P. Manneville and M. Shimizu, *Entropy* **22**, 1348 (2020).
- [45] D. Barkley and L. S. Tuckerman, *Physical review letters* **94**, 014502 (2005).
- [46] S. Toh and T. Itano, *Journal of Fluid Mechanics* **481**, 67 (2003).
- [47] Y. Duguet, O. Le Maitre, and P. Schlatter, *Physical Review E* **84**, 066315 (2011).

- [48] X. Xiao and B. Song, *Journal of Fluid Mechanics* **883** (2020).
- [49] H. Ji, M. Burin, E. Shartman, and J. Goodman, *Nature* **444**, 343 (2006).
- [50] D. Xu, A. Varshney, X. Ma, B. Song, M. Riedl, M. Avila, and B. Hof, *Proceedings of the National Academy of Sciences* **117**, 11233 (2020).

ACKNOWLEDGEMENTS

We thank Yohann Duguet for helpful discussions and Baofang Song for supplying the code for the direct numerical simulations.

Supplementary Information

Vasudevan Mukund, Chaitanya Paranjape, Michael Philip Sitte, and Björn Hof*
IST Austria

EXPERIMENTS

Experimental Setup

The experiments are carried out in a large aspect ratio channel which consists of two plates separated by a narrow gap of $2h = 1 \pm 0.03$ mm (Fig.S1). The bottom plate is a 10 mm thick, finely polished aluminum plate, while the top is 10 mm thick float glass. The gap is maintained by 1mm thick steel strips, which are clamped between the glass and steel plates and form the side-walls of the set up. The size of the channel is $(L_x; L_y; L_z) = (4000h; 2h; 490h)$, where L_x , L_y and L_z are lengths in the streamwise, wall-normal and spanwise directions respectively. The working fluid is water, supplied from a continually overflowing reservoir, which is kept at the height of 21 m above the channel. The water level in the reservoir is maintained within ± 2 cm, ensuring the pressure-head that drives the flow to be constant within $\pm 0.1\%$. The excess pressure drop due to an isolated stripe is less than 0.2% of the total pressure head and hence the flow rate remains constant during stripe decays or splittings within a fraction of a percent.

Prior to entering the channel the water passes through a settling chamber including a porous barrier which breaks up large eddies. It then enters the channel proper via a convergence with an area ratio of 90:1. Unless perturbed, the flow in the channel remains laminar over the entire Reynolds number range investigated here.

The water temperature is measured just before the convergence by a precision resistance thermometer. The viscosity of the water ν is then determined using a fit to standard temperature-viscosity tables for water. The flow rate is measured by a magnetic flowmeter (ABB) installed in the main supply pipe leading to the channel, from which the bulk velocity u_{bulk} is calculated.

To permit comparison with earlier studies, quantities are non-dimensionalised with the length scale h (half-gap) and 1.5 times the bulk velocity u_{bulk} (which corresponds to the centre line velocity of the laminar flow at the same mass flow rate).

Perturbation techniques

To study the evolution of isolated turbulent stripes, an effective mechanism to generate them is needed. For $Re > 900$, almost any standard perturbation mechanism (static obstacle, moving obstacle, jets injected through one or more holes in the channel wall) can efficiently trigger turbulence. Although for the lower Re range studied here ($600 < Re < 900$), many of these do not work anymore, two methods were found to be efficient in generating isolated stripes. In one, perturbing the flow over a certain minimum span-wise ($\sim 20h$) width successfully triggered stripe turbulence. In the present study we realized this by placing a ferromagnetic obstacle $100h$ downstream of the inlet which can be actuated by impulsively moving an externally placed magnet across the upper channel surface. This extended perturbation generates a seed which evolves into a stripe.

In the other method, a stripe is generated at a Re higher than the target Re , where stripes are easily generated by a localized or extended perturbation (as described above). Next the Reynolds number was quenched to the target value. This was accomplished with a bypass loop in the supply pipe leading to the channel, which was normally closed by a solenoid valve. Prior to triggering the stripe, the flow-rate is adjusted to the target Re , with the bypass valve being closed. The valve is then opened, reducing the resistance in the supply pipes, and hence increasing the flow-rate and hence the Re by around 100 - 150. After the stripe is triggered at this higher Re , it is allowed to develop for a time of around $300h/u_{bulk}$. Subsequently the solenoid valve is closed, quenching the flow down to the target Re . Readings are taken after a further $250h/u_{bulk}$ to allow the flow to adjust to the change in Re . In comparison to the quench, the generation of stripes by an extended perturbation becomes increasingly inefficient for the lowest Re studied here ($Re < 700$).

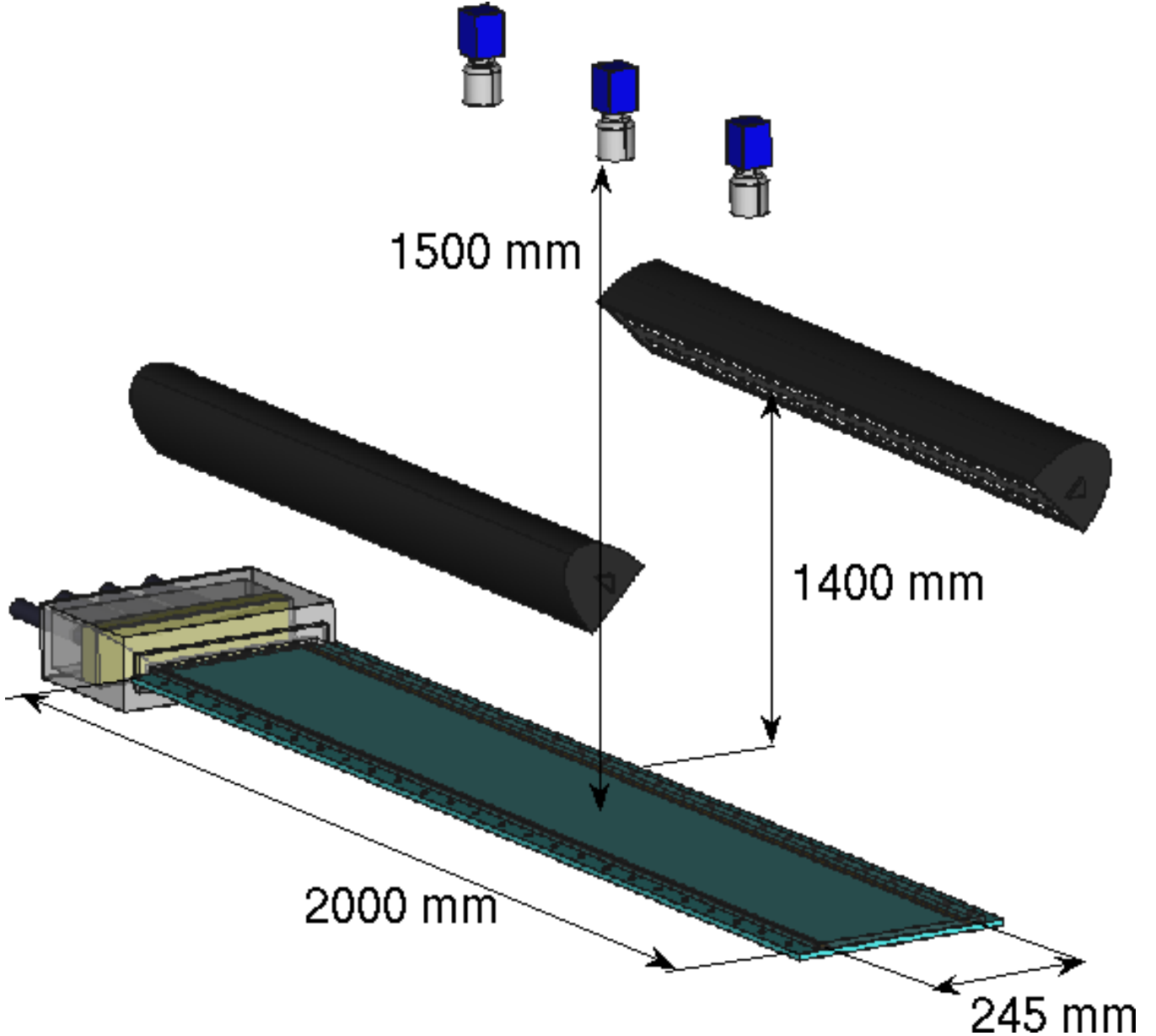


FIG. 1. The Channel set-up

Flow visualization

The channel is illuminated with the help of LED lights installed parallel to the channel axis on both sides of the channel, approximately 1.4 m above it. The flow was visualized using reflective flakes $10 - 40\mu$ in size (Eckart SYMIC C001 reflective mica particles). These flakes tend to orient along the shear and hence allow to clearly distinguish turbulent from laminar regions. The flow structures are monitored in the test section with the help of three 4 Mpixel 100Hz cameras placed at a distance around 1.5 m above the channel. In order to allow time for the quench or the decay of initial transients, the test section is located some distance downstream of the channel entrance, and flows are recorded from $1500h$ downstream of the channel entrance till $500h$ before the channel exit. The combined view-field of the three cameras is $2000h \times 490h$. To monitor the evolution of a stripe, images are captured by the cameras at a set frequency, with the three cameras being simultaneously triggered each time by a TTL signal.

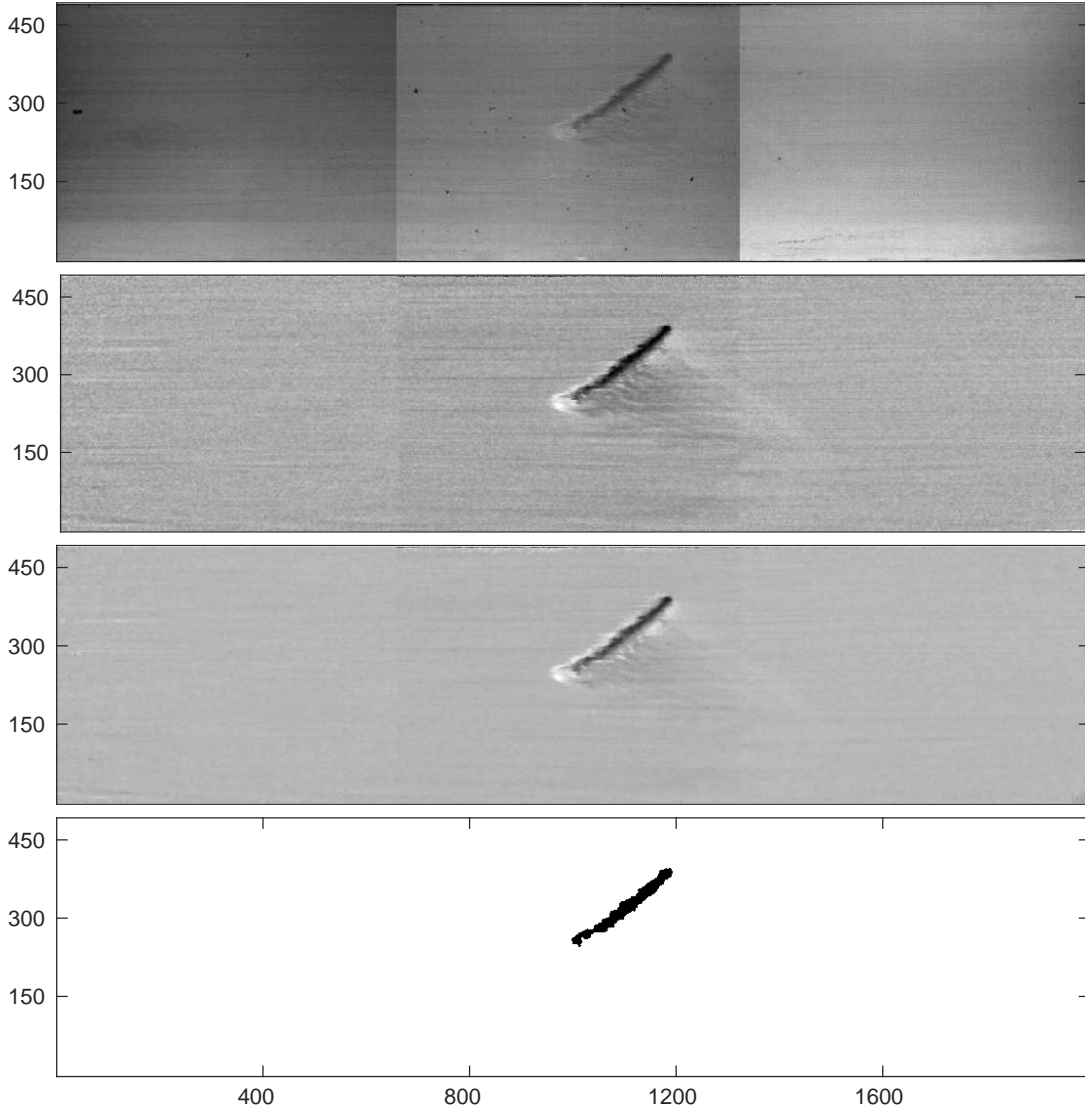


FIG. 2. Image Processing (a) Raw image from the cameras stitched together showing an isolated stripe. (b) Background subtracted image. (c) Image after filtering and sharpening. (d) Binary image after thresholding

The images of the three cameras are merged to capture the flow field in the entire test section (Fig.S2a) and further processed by subtracting images of the laminar background flow (Fig.S2b). Images are next low-pass filtered using a Wiener filter with a 5×5 pixel mask. This is sharpened using unsharp masking in order to increase the contrast between the edges of the stripe and its surroundings (Fig.S2c). This can be further used for extracting quantities of interest. For instance, in order to determine the area occupied by a stripe, a simple threshold is subsequently applied to create a binary image, shown in Fig.S2d. The pixel count of the black area is then the area occupied by the turbulent stripe. For a reasonable range of parameters used in the image processing (e.g. the threshold for binarizing the image), there is only a minor variation in derived quantities such as the area of the turbulent stripe. More importantly such changes do not affect the value of the critical point or the lifetime distributions etc.

The growth rate of turbulence was estimated as follows. For each Re , around 1000 stripes are generated. Each stripe is considered at a definite time after the perturbation, its area determined and then an average found over all the stripes at that Re at the same time, thus yielding an ensemble average of the turbulent fraction at that time. Doing this for different times gives the evolution of the turbulent fraction as a function of time, from which the growth rate is determined. In flows where the proliferation and decay of turbulence are memoryless, the typical time scales of these processes are well defined and the critical point is then determined as the Re where these timescales are in

balance. By contrast, here, the critical point is determined as the Re where the growth rate changes from negative to positive.

Stripe splitting

Small stripe segments are randomly shed from the stripe's upstream (trailing) edge. One such event each is shown by red circles in Fig 3(a) and (b) of the main paper. At low Re ($\lesssim 675$), such pieces typically decay. At larger Re however, some of these develop into an independent stripe parallel to, and upstream of the original parent stripe. An example of this splitting process is shown in Fig.S3.



FIG. 3. A sequence of three images at $Re = 750$ showing stripe splitting. Consecutive images are 800 advective time units apart. A portion at the upstream tip (trailing edge) breaks off (b) and grows into an independent stripe upstream of the original one (c)

NUMERICAL SIMULATIONS

The numerical simulations in the present study are carried out using a modified version of the spectral code *openpipeflow* [1], which was adapted to simulate channel flow [2] in a rectangular box.

X', Y', Z' are the streamwise, spanwise and wall-normal directions, with the associated unit vectors being e'_x, e'_y, e'_z respectively. When scaled with half channel height h and centre-line velocity U_{cl} of the parabolic profile with the same mass flux, the laminar base flow can be expressed as $\mathbf{U} = (1 - y^2)\mathbf{e}_{x'}$, and the Navier-Stokes equations for the fluctuating components (\mathbf{u}, p) around base flow \mathbf{U} take the form

$$\frac{\partial \mathbf{u}}{\partial t} + (\mathbf{u} \cdot \nabla) \mathbf{u} + (\mathbf{u} \cdot \nabla) \mathbf{U} + (\mathbf{U} \cdot \nabla) \mathbf{u} = -\nabla p + \frac{1}{Re} \nabla^2 \mathbf{U} + \frac{1}{Re} \nabla^2 \mathbf{u} + \mathbf{f}(t) \quad (1)$$

$$\nabla \cdot \mathbf{u} = 0 \quad (2)$$

Here, the Reynolds number is defined as $Re = U_{cl}h/\nu$, where ν is the kinematic viscosity of the fluid. $\mathbf{f}(t) = f(t)\mathbf{e}_{x'}$ is a time-dependent forcing term that represents an imposed streamwise pressure gradient. The mass flux in the streamwise direction $\mathbf{e}_{x'}$ is kept constant by changing the amplitude of the forcing term at every time-step.

No slip boundary conditions are imposed on the domain walls

$$\mathbf{u}(x, \pm 1, z) = 0 \quad (3)$$

Computational domain

The computations are carried out in a rectangular box shaped domain which can be tilted with respect to the streamwise direction [3, 4] at an angle θ , where $0^\circ \leq \theta \leq 90^\circ$.

The sides of the rectangular box x and z have associated unit vectors \mathbf{e}_x and \mathbf{e}_z respectively. The usual streamwise, wall-normal and spanwise directions have following relation with the unit vectors associated with the domain directions.

$$\hat{\mathbf{e}}_{x'} = \cos \theta \hat{\mathbf{e}}_x + \sin \theta \hat{\mathbf{e}}_z \quad (4)$$

$$\hat{\mathbf{e}}_{z'} = -\sin \theta \hat{\mathbf{e}}_x + \cos \theta \hat{\mathbf{e}}_z \quad (5)$$

$$\hat{\mathbf{e}}_{y'} = \hat{\mathbf{e}}_y \quad (6)$$

A constant mass flux is maintained in the streamwise direction and periodic boundary conditions are imposed on the faces normal to \mathbf{e}_x and \mathbf{e}_z .

$$\begin{aligned} \mathbf{u}(x, y, z) &= \mathbf{u}(x + L_x, y, z) \\ \mathbf{u}(x, y, z) &= \mathbf{u}(x, y, z + L_z) \end{aligned} \quad (7)$$

where, L_x and L_z are lengths of the domain in the x and z directions respectively.

The solver uses Fourier modes in the two periodic directions and finite-difference in the wall-normal direction. The velocity field is decomposed as

$$\mathbf{u}(x, y, z, t) = \sum_{k=-K}^K \sum_{m=-M}^M \hat{\mathbf{u}}_{k,m}(y, t) e^{i(\alpha k_x x + \beta m_z z)} \quad (8)$$

where k and m are Fourier modes in the x and z directions respectively, $\alpha = 2\pi/L_x$, $\beta = 2\pi/L_z$. L_x, L_z are the lengths of the domain in x and z directions respectively. The time integration is performed using a second-order backward differentiation for linear terms and the Adam-Bashforth method for the nonlinear terms.

The evolution of the stripes is monitored by defining a scalar observable - perturbation kinetic energy $E(t)$ defined as

$$E(t) = \frac{1}{L_x L_y L_z} \int_{-1}^1 \left(\int_0^{L_z} \int_0^{L_x} |\mathbf{u}|^2 dx dz \right) dy. \quad (9)$$

Large domain with $\theta = 0^\circ$

A fully localized stripe can be simulated only in a large enough domain. We studied the lifetimes of the stripes at $Re = 620$ in a square domain with no tilt i.e. $\theta = 0^\circ$ with size $(L_x, L_y, L_z) = (400, 2, 400)$ and resolution $(N_x, N_y, N_z) = (1536, 64, 1536)$.

The resolution used is sufficient for the simulations at $Re = 620$. The initial conditions for the lifetime study are uncorrelated snapshots from simulations at $Re = 700$ in the same domain. The lifetimes are determined by setting an appropriate cut-off on the perturbation kinetic energy. Once the perturbation KE falls below this threshold, the stripe is considered to have decayed. However, unlike the case of the partially localized stripes, there is no plateau in the energy before the decay. Rather the KE decays gradually (Fig.2b in the main paper). Hence, the lifetimes depend significantly on the threshold. The lifetimes for different threshold values are shown in Fig.S4. Though the lifetimes do depend on the threshold, the qualitative behavior remains the same, exhibiting a non-exponential decay of survival probabilities.

Tilted domain

A partially localized stripe i.e. a stripe localized only in one direction and periodic in other direction is simulated in a rectangular domain tilted with respect to the streamwise direction at an angle of $\theta = 45^\circ$. This tilt angle also

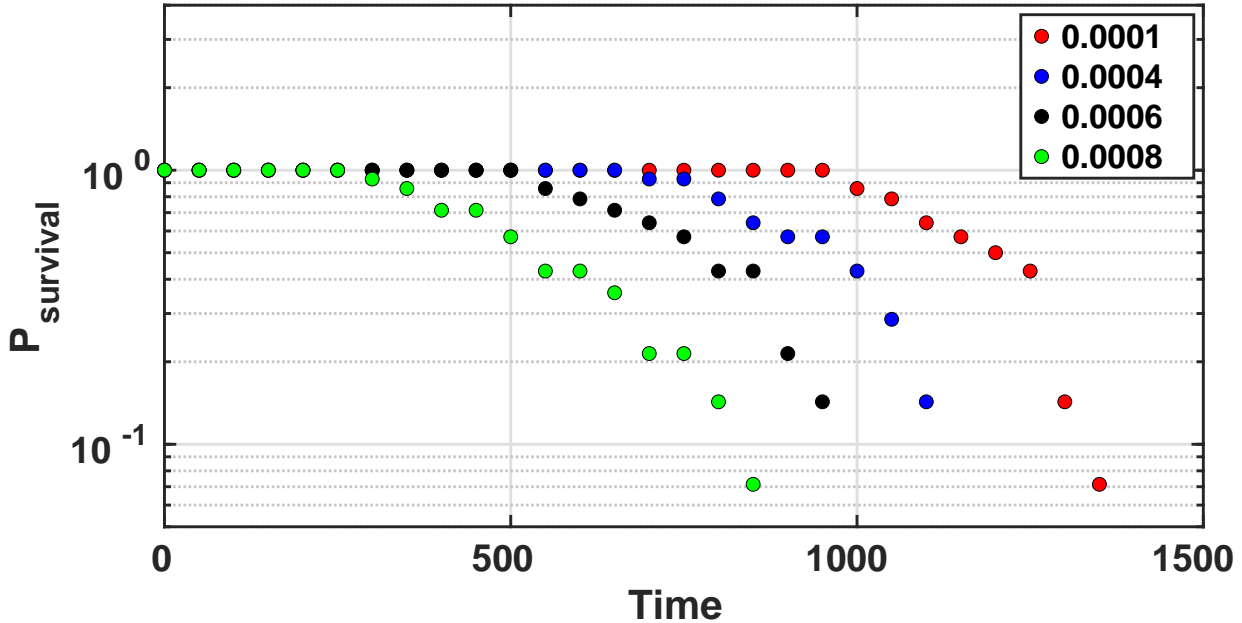


FIG. 4. Survival probability of fully localised stripes at $Re = 620$. For different values of cutoffs used to determine lifetimes, the qualitative behaviour does not change.

corresponds to the stripe angle with respect to the streamwise direction [5] and the angle of tilt chosen here agrees with the tilt angle of the stripes observed in the experiments and reported in [6].

The domain size is $(L_x, L_y, L_z) = (30, 2, 100)$ with resolution $(N_x, N_y, N_z) = (256, 49, 768)$. The initial conditions for the lifetime study are taken from uncorrelated snapshots from simulations at $Re = 600$. The stripe is considered to have decayed when the energy of fluctuations drops below a selected cutoff value e.g. $E = 0.01$. Due to the rather clear plateau in energy before decay, the results do not strongly depend on the cut off chosen (see Fig.2 in the main paper).

* bhof@ist.ac.at

- [1] A. P. Willis, *SoftwareX* **6**, 124 (2017).
- [2] X. Xiao and B. Song, *Journal of Fluid Mechanics* **883** (2020).
- [3] D. Barkley and L. S. Tuckerman, *Physical review letters* **94**, 014502 (2005).
- [4] L. S. Tuckerman, T. Kreilos, H. Schröbsdorff, T. M. Schneider, and J. F. Gibson, *Physics of Fluids* **26**, 114103 (2014).
- [5] C. S. Paranjape, Y. Duguet, and B. Hof, *Journal of Fluid Mechanics* **897** (2020).
- [6] J. Tao, B. Eckhardt, and X. Xiong, *Physical Review Fluids* **3**, 011902 (2018).